

# The Evolution of Embedded Star Clusters

F. I. Pelupessy<sup>1\*</sup> and S. Portegies Zwart<sup>1</sup>

<sup>1</sup>*Leiden Observatory, Leiden University, PO Box 9513, 2300 RA, Leiden, The Netherlands*

## ABSTRACT

We study the evolution of embedded clusters. The equations of motion of the stars in the cluster are solved by direct N-body integration while taking the effects of stellar evolution and the hydrodynamics of the natal gas content into account. The gravity of the stars and the surrounding gas are coupled self consistently to allow the realistic dynamical evolution of the cluster. While the equations of motion are solved, a stellar evolution code keeps track of the changes in stellar mass, luminosity and radius. The gas liberated by the stellar winds and supernovae deposits mass and energy into the gas reservoir in which the cluster is embedded. We examine cluster models with 1000 stars, but we varied the star formation efficiency (between 0.05-0.5), cluster radius (0.1-1.0 parsec), the degree of virial support of the initial population of stars (0-100%) and the strength of the feedback. We find that an initial star fraction  $M_*/M_{\text{tot}} > 0.05$  is necessary for cluster survival. Survival is more likely if gas is not blown out violently by a supernova and if the cluster has time to approach virial equilibrium during out-gassing. While the cluster is embedded, dynamical friction drives early and efficient mass segregation in the cluster. Stars of  $m \gtrsim 2 M_{\odot}$  are preferentially retained, at the cost of the loss of less massive stars. We conclude that the degree of mass segregation in open clusters such as the Pleiades is not the result of secular evolution but a remnant of its embedded stage.

**Key words:** star clusters – star formation – numerical simulations: hydrodynamic, N-body

## 1 INTRODUCTION

The loss of gas that signifies the end of star formation in an embedded proto-cluster may also cause the young cluster to dissolve (Hills 1980; Lada et al. 1984). The energy output from all the massive stars typically exceeds the total binding energy of the embedded star cluster. The survivability of the cluster therefore depends on the efficiency with which the radiative, thermal and mechanical energy of the stellar outflows couple to the inter-cluster gas (and as long as this energy is not carried away by outflows, Dale et al. 2005). The time scale on which gas is removed from the embedded cluster (and any spatial dependence of this process) affects the mass and number of stars in the surviving cluster, but also its degree of mass segregation and the density profile. The parameters that strongly affect the outcome of the out-gassing phase are the star formation efficiency (SFE, which by itself could depend on feedback processes, Dale & Bonnell 2008; Vázquez-Semadeni et al. 2010), the efficiency of the radiative coupling and the pop-

ulation of the most massive stars in the proto cluster. Traditionally the critical value for the star formation efficiency is taken to be  $\text{SFE} \approx 0.5$  on the basis of virial arguments (e.g. Hills 1980; Mathieu 1983), but later work showed that SFEs as low as 0.1 can still lead to bound clusters, albeit with a reduced mass (Lada et al. 1984; Adams 2000; Geyer & Burkert 2001; Baumgardt & Kroupa 2007; Goodwin 2009). Observed star formation efficiencies fall into the range 0.05-0.3 (Williams & McKee 1997). It is therefore expected that clusters must experience considerable structural disruption before settling.

From an observational point of view, the number of embedded clusters is too high with respect to the number of observed gas-free clusters. Within the solar neighborhood the observed distribution of cluster ages suggests that more than 95% of embedded clusters dissolve into the field within 100 Myr (Lada & Lada 2003). The disruption of young clusters by the loss of the remnant gas provides a natural explanation, although alternatively the young clusters may be disrupted by tidal forces (Elmegreen & Hunter 2010; Kruijssen 2011). In this scenario it is not the internal evolution of the cluster that disrupts the structure, but

\* E-mail: pelupes@strw.leidenuniv.nl

tidal shocks from passing gas clouds (see also Gieles et al. 2006). In order to find out what the relative contribution is from these two processes we need to understand the effects of gas loss quantitatively. Ultimately the modeling of the formation of cluster populations is needed to interpret the observations as they play a pivotal role in galaxy evolution studies (e.g. Schweizer & Seitzer 1998; Larsen et al. 2001; Bastian et al. 2005). Without understanding early cluster evolution we cannot relate the young cluster populations (which are easily observed to large distances) to the older stars and the stellar population in the field. Contrary to stars, clusters are sensitive to the galactic environment and if we would understand the starting conditions of the cluster population we could search for the signatures of later galactic evolutionary events such as galaxy mergers and major gas inflows.

The expulsion of gas from young clusters has been studied by applying a time-dependent background potential within which the N-body system is integrated (Lada et al. 1984; Geyer & Burkert 2001; Boily & Kroupa 2003b; Baumgardt & Kroupa 2007; Chen & Ko 2009; Goodwin 2009; Smith et al. 2011). The time scale for out-gassing can then be controlled rather straightforwardly by the decay time scale of the background potential. This parametrization allows the study of different mass loss scenarios without the complications of modeling gas dynamics and feedback. Geyer & Burkert (2001) examined the evolution of a cluster both using the external potential approximation and for a limited set of combined N-body/SPH simulations (using simplified feedback prescriptions). They found general agreement between the simulations with a dynamic gas component and a static gas potential, and found that relatively long timescales of gas loss are necessary for clusters to survive. To reconcile observed low SFEs with their simulations, they point out that although the global SFE may be low in a star forming region, locally the SFE may be much higher and allow for bound clusters (also Adams 2000). Furthermore they proposed sub-virial stellar velocity dispersions as an alternative possibility (see also Goodwin 2009).

Baumgardt & Kroupa (2007) conducted a grid of simulations in which they varied the SFE, gas expulsion timescale and external tidal field. They confirmed that clusters with a SFE as low as 10% could survive, although they found a strong dependence on the timescale (parametrized by an e-folding time) on which the gas potential was removed. Surviving clusters had expanded drastically; for SFEs of around 25% this was a factor 3-4, nearly independent of the gas loss timescale. The velocity distributions became strongly radially anisotropic in the cases where the gas was removed on timescales much shorter than a crossing time.

It has become clear from observations and simulations that young stars start out in a structured, clumpy, state (Lada & Lada 2003; Portegies Zwart et al. 2010). Recent work examining hierarchical cluster formation (Smith et al. 2011; Kruijssen 2011) suggests that sub-clustering increases the survivability. If clusters tend to be born sub-virial, they can survive even the loss of large fractions of intercluster gas, in which case the SFE may not be a good indicator of survivability. Smith et al. (2011) (see also Kruijssen 2011) found that the local gas fraction immediately prior to gas loss is a better diagnostic for the cluster survival than the global

SFE. By studying sub-clusters in hydrodynamical simulations of collapsing molecular clouds where sink particles represent stars, Kruijssen (2011) found that the environment around  $\sim 40 M_{\odot}$  clumps has a gas content of only 10%-30%. The relative lack of gas resulted from the accretion of gas onto stars (which depletes the gas reservoir) and the shrinkage of the virialized sub clumps (because the dynamics of these clumps decouples from the gas dynamics). For such low gas fractions no major disruption is expected when feedback clears the gas. On the larger scales gas fractions are still considerably higher. Kruijssen (2011) argues that a similar effect will also cause the larger scales to become gas poor, if sufficient time elapses before the onset of feedback. However, during this delay the different clumps would merge and relax, evolving from the highly structured state towards a smooth density distribution (this was also the case for the simulations for Smith et al. (2011), where this happened within 3 Myr). The conditions at this stage would determine the outcome with regard to the final survival, and by this stage the local depletion of gas by accretion may no longer be present.

The above studies have expanded considerably on the simple picture where clusters dissolution is determined solely or mainly by the single SFE parameter. Clusters seem to have a number of ways in which they can resist the disruptive effect of the loss of their gas content: disruption is less or absent if the gas loss occurs on timescales longer than the crossing time or if the gas loss is delayed enough that shrinking due to relaxation processes can occur. On the other hand, if the stellar population of the cluster forms sub-virialized, some of the stars in the cluster can evolve into low energy orbits and these will not be ejected as easily, even if the SFE is low. Hence, to constrain the disruption process of clusters, we need to employ numerical simulations to unravel various complex physical processes at work. The determination of the gas loss timescale and the spatial distribution requires careful modeling of the response of the parent gas cloud to the mechanical luminosity of the young stars using realistic stellar evolution models (the feedback from radiation, stellar winds and supernovae will be neither constant nor instantaneous) coupled to a hydrodynamic code. Following the evolution of the stellar component requires that the stellar dynamics be resolved in high detail, including two-body relaxation processes. For this an N-body code for collisional gravitational dynamics is necessary. The relaxation processes also require that a realistic initial mass function (IMF) is adopted, which is also required for the stellar evolution modeling. The stellar dynamics and hydrodynamics code must be mutually coupled as they feel each other's gravity. Here we will present simulations that were conducted using the newly developed Astrophysical Multi-purpose Software Environment (AMUSE; Portegies Zwart et al. 2009; Pelupessy et al. 2011) that couple stellar dynamics of young clusters with the gas dynamics using realistic feedback physics. Using these simulations we will explore idealized but realistic scenarios of gas loss and analyze the trends with SFE, feedback strength and the dependence on the initial distribution. We will start by presenting the AMUSE package, the solvers and initial conditions of the runs we conducted in Section 2. The results are presented in Section 3 and discussed in 4. We summarize our main conclusions in Section 5.

## 2 METHOD

We study the evolution of embedded star clusters using a hybrid simulation environment. Our models combine the effects of the self-gravity of the stars, their nuclear evolution and the hydrodynamics of the gas. The latter has contributions of the primordial gas content and of the gas liberated by the stars in stellar winds and supernovae. The various simulation ingredients are coupled self-consistently using AMUSE (Portegies Zwart et al. 2009; Pelupessy et al. 2011). In the code, a script in the AMUSE framework, we couple a collisional N-body code, a Smoothed Particles Hydrodynamics (SPH) code and a stellar evolution code together to form a complete description of the physics that govern the evolution of an embedded star cluster. The integration of the equations of motion of the stars was conducted using the fourth-order predictor-corrector Hermite N-body solver phiGRAPE (Harfst et al. 2007). The dynamics of the gas was resolved using the SPH code Gadget-2 (Springel 2005). For the gravitational coupling between the stars and the self-gravity of the gas we used the gravitational treecode Octgrav (Gaburov et al. 2010). The stars in our simulations were evolved using parametrized stellar evolution tracks (using the SSE code, Hurley et al. 2000). Each of the numerical simulation codes is embedded in the AMUSE framework, and the code that realizes the self-consistent coupling between each of the physical sub-domains turns out to be a relatively straightforward script. Within the AMUSE environment the individual sub-solvers are referred to as *community codes*. The algorithms used by these community codes remain the same as described by their respective authors. The codes are written in different languages and have a wide range of programming styles. Because the adopted community codes are untouched, we will not further explain their operations, but simply refer the reader to the appropriate literature. The AMUSE framework that stitches each of the community codes together is one of the major ingredients that enables us to perform a consistent coupling between the various scales and physical domains. Therefore we give a short overview of the framework in the following section.

### 2.1 AMUSE

The AMUSE environment that we use to conduct the simulations is a package that allows astrophysical codes from different domains to be combined to conduct numerical experiments (see Pelupessy et al. 2011 for a more complete description). AMUSE is a development of the Multi-physics and Multi-scale Software Environment (MUSE, Portegies Zwart et al. 2009) and is freely available for download<sup>1</sup>. The fundamental idea of AMUSE is the abstraction of the functionality of simulation codes into physically motivated interfaces that hide the complexity and numerical implementation of the codes. AMUSE presents the user with building blocks that can be combined into applications and numerical experiments. The binding language that stitches the codes together is Python<sup>2</sup>, as the focus in these high level interactions is not so much performance (the computational cost being concentrated in the component codes) but

on algorithmic flexibility and ease of programming to allow rapid prototyping.

An AMUSE application consists, roughly speaking, of a *user script*, one or more *community modules* and the *community code* (fig 1). The user script specifies the initial conditions and selects the simulation codes. The relationships between the community codes define the solver and for our case we construct a combined N-body/hydrodynamic solver using a direct N-body code and an SPH solver. The setup and communication with a community code is handled by the community module. This consists of an MPI<sup>3</sup> based communication interface with the code as well as unit handling facilities and an object oriented data model. The heart of an AMUSE application consists of the solvers employed: here these are the Gadget-2 SPH code (Springel 2005), the PhiGRAPE Hermite N-body code (Harfst et al. 2007), the tree gravity code Octgrav (Gaburov et al. 2010) and the stellar evolution code SSE (Hurley et al. 2000).

### 2.2 The combined solver

An overview of the calling sequence of our combined solver is given in figure 2. It consists of a combined integrator for coupled gas/gravitational dynamics systems and a feedback prescription for mechanical energy input.

#### 2.2.1 BRIDGE integrator

The BRIDGE integrator (Fujii et al. 2007) provides a semi-symplectic mapping for the gravitational evolution in cases where the dynamics of a system can be split in different regimes. A typical application would be a dense star cluster in a galaxy where the internal dynamics of the former evolves on a relatively short timescale compared to the dynamics of the host galaxy. A similar idea was applied by Saitoh & Makino (2010) by splitting the gravitational and hydrodynamic evolution operators for simulating gas-rich galaxy mergers. They implemented the algorithm in a single monolithic code, whereas we adopt the concept of operator splitting within AMUSE to couple different codes. In our case we will also employ a split between the gravitational evolution operator of the stellar component (which is governed by collisional dynamics) and the hydrodynamic evolution operator (governed by SPH dynamics).

The BRIDGE formulation is derived by applying the splitting method developed in planetary dynamics (Wisdom & Holman 1991; Duncan et al. 1998) to the Hamiltonian

$$H = \sum_{i \in A \cup B} \frac{p_i^2}{2m_i} + \sum_{i \neq j \in A \cup B} \frac{Gm_i m_j}{\|r_i - r_j\|} \quad (1)$$

of a system of particles which consists of subsystems A and B by dividing the Hamiltonian into three parts

$$H = \sum_{i \in A} \frac{p_i^2}{2m_i} + \sum_{i \neq j \in A} \frac{Gm_i m_j}{\|r_i - r_j\|} + \sum_{i \in B} \frac{p_i^2}{2m_i} + \sum_{i \neq j \in B} \frac{Gm_i m_j}{\|r_i - r_j\|} + \quad (2)$$

<sup>1</sup> [www.amusecode.org](http://www.amusecode.org)

<sup>2</sup> [www.python.org](http://www.python.org)

<sup>3</sup> <http://www.mpi-forum.org/>

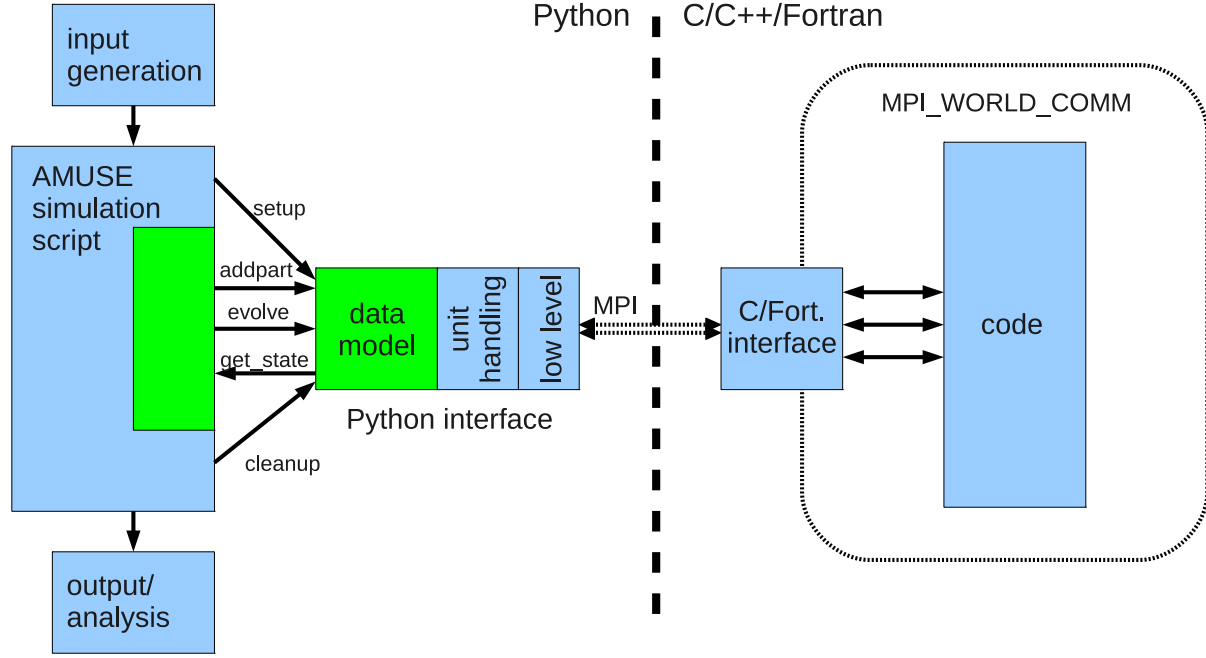


**Figure 1.** The AMUSE interface design. This diagram represents the way in which a community code (“code”) is accessed from the AMUSE framework. The code has a thin layer of interfaces functions in its native language which communicate through an MPI message channel with the python host process. On the python side the user script (“AMUSE simulation script”) only accesses generic calls (“setup,” “evolve” etc.) to a high level interface. This high level interface calls the low level interface functions, hiding details about units and the code implementation (together these form the *community module* of the code). The communication through the MPI channel does not interfere with the code’s own parallelization.

$$\sum_{i \in A, j \in B} \frac{Gm_i m_j}{\|r_i - r_j\|} = H_A + H_B + H_{A,B}^{\text{int}} \quad (3)$$

where  $H_A$  and  $H_B$  are the Hamiltonians of subsystems A and B respectively and the cross terms are collected in  $H^{\text{int}}$ . The formal time evolution operator of the system can then be written as ( $\mathbb{H}$  is the Hamiltonian vector field corresponding to a Hamiltonian  $H$ ):

$$\begin{aligned} e^{\tau \mathbb{H}} &= e^{\tau/2 \mathbb{H}^{\text{int}}} e^{\tau(\mathbb{H}_A + \mathbb{H}_B)} e^{\tau/2 \mathbb{H}^{\text{int}}} \\ &= e^{\tau/2 \mathbb{H}^{\text{int}}} e^{\tau \mathbb{H}_A} e^{\tau \mathbb{H}_B} e^{\tau/2 \mathbb{H}^{\text{int}}}. \end{aligned} \quad (4)$$

The  $e^{\tau/2 \mathbb{H}^{\text{int}}}$  operator represents momentum kicks because  $H^{\text{int}}$  depends only on the position of the particles. The operator  $e^{\tau(\mathbb{H}_A + \mathbb{H}_B)}$  splits into secular evolution operators, because  $H_A$  and  $H_B$  are independent. The evolution of the total system over a time step  $\tau$  can subsequently be calculated from the mutual forces exerted by systems A on B and by kicking the momenta for time  $\tau/2$ , after which the two systems are evolved in isolation for a time  $\tau$ , after which the time step is finished by another mutual kick. This procedure is beneficial if, for example, the time step allowed by the mutual interactions is considerably longer than that required by the internal dynamics of the component systems, or if the gravitational dynamics of the two sub-systems need different solving strategies.

Within AMUSE we view the various gravitational and

hydrodynamical codes as implementations of the time evolution operators  $e^{\tau \mathbb{H}}$  (for this the interface specification provides an `evolve` function). The momentum kicks are easy and reasonably fast to implement within the framework in Python once the forces are known, and for this the gravitational dynamics interface provides utility functions to query the gravitational forces at arbitrary positions.

The gas dynamical SPH evolution can also be derived from a Hamiltonian formalism and thus the above directly carries over to a split between purely gravitational and SPH particles. The application of a BRIDGE type integrator to SPH is computationally efficient if the time step requirement for the hydrodynamics is more stringent than for the gravitational dynamics (which generally is the case, Saitoh & Makino 2010). Our application within AMUSE has the additional benefit that we can easily swap in and out different gravitational solvers and SPH codes, even if they use completely different algorithms (such as in our case a direct Hermite code and a tree based SPH integrator).

For validation, the resulting combined gravitational-hydrodynamical solver was checked in problems which could also be calculated using a monolithic SPH code. For this a number of static and dynamic test runs were conducted and the results were verified to be consistent with runs conducted purely with Gadget-2. First, in order to check that the alternation of hydrodynamic and gravitational evolution operators does not introduce artifacts in cases where grav-

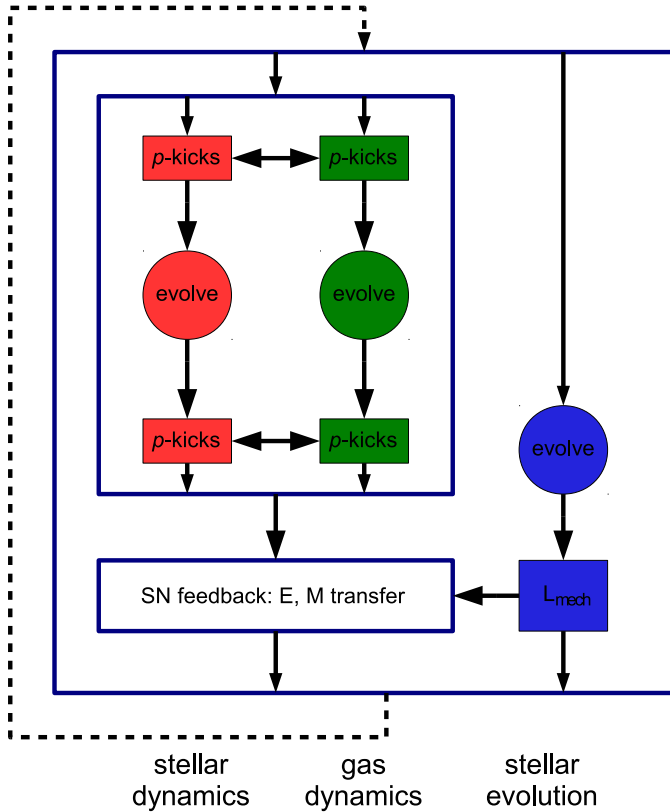


**Figure 2.** The AMUSE gravitational/hydro/stellar evolution integrator. This diagram shows the calling sequence of the different AMUSE elements in the combined gravitational/hydro/stellar solver during a time step of the combined solver. Circles indicate calls to the (optimized) component solvers, while rectangles indicate parts of the solver implemented in Python within AMUSE.

itional and hydrodynamic forces are in equilibrium, we conducted static tests where the ability of the code to maintain a Plummer sphere in equilibrium was examined. Tests were conducted using different particle numbers (10k-200k) and gas fractions (50% and 100%). As a dynamic test we conducted the *Evrard* (Evrard 1988) collapse tests with the combined AMUSE solver. Both the dynamic and static tests showed satisfactory results compared to a conventional integrated code (Pelupessy et al. 2011).

### 2.2.2 Feedback prescription

In our calculations we include feedback from stellar wind and supernovae. Radiative processes are not taken into account self-consistently, even though the ionizing radiation from massive stars can drive violent outflows (Rodríguez-Gaspar et al. 1995; Diaz-Miller et al. 1998; Dale et al. 2005); the relative strength of the radiative feedback is expected to be of the same order of magnitude as the mechanical feedback from stellar winds (Fall et al. 2010), which is included in our calculations.

Given these uncertainties (and the fact that we do not explicitly include radiative feedback) we have chosen to simplify the modeling by taking an adiabatic equation of state and not solving the thermal and chemical balance of the gas. We parametrize the energy budget in the absence of radia-

tive losses with a coupling strength parameter  $f_{fb}$ , which is the fraction of the total supernova and wind energy output that ends up as thermal energy in the ISM. The relative strength of the feedback is of the order of a few percent, the rest is radiated away (Wheeler et al. 1980; Silich et al. 1996; Freyer et al. 2003, 2006).

For the actual implementation of the feedback within our model we calculate the mechanical luminosity  $L_{\text{mech}} = \dot{M}v_{\infty}^2$  of the stars, from parametrized mass loss rates and terminal wind velocities (Leitherer et al. 1992; Prinja et al. 1990). The mass liberated in the stellar wind of the stars is subsequently injected into the cluster medium. All gas particles have the same mass  $m_{\text{gas}}$  throughout the simulation. The gas particles are released at rest relative to the star releasing them in a sphere with a radius equal to the smoothing length of the gas particles around the star, and the stellar mass is reduced accordingly. A consequence of this prescription is that each star loses mass in discrete steps of at least  $m_{\text{gas}}$ . For the runs presented here the  $m_{\text{gas}}$  varies between  $\approx 3 \times 10^{-3} - 6 \times 10^{-2} M_{\odot}$ . As a consequence the stellar wind feedback will exhibit some discreteness noise if the mass loss rate of a star is lower than  $\sim 7.5 \times 10^{-8} - 1.5 \times 10^{-6} M_{\odot}/\text{yr}$  (Note that the feedback will still be approximately isotropic if a low number of particles is released due to the SPH smoothing). We verified that the results of our simulations with respect to the stellar response converges and therefore are not affected by this discretization. For the most active wind phases ( $\dot{M} \gtrsim 10^{-5} M_{\odot}/\text{yr}$ ) the feedback prescription leads to 10s-100s of particles released per timestep and a smooth wind (see section 3). The internal energy  $u$  of the gas lost by the star is calculated from the total energy output of the star  $E_{\text{mech}}$  since the last discrete mass loss event:

$$u = f_{\text{fb}} \frac{E_{\text{mech}}}{m_{\text{grav}} - m_{\text{evo}}} = f_{\text{fb}} \int_{t_{\text{last}}}^t L_{\text{mech}} / (m_{\text{grav}} - m_{\text{evo}}) dt \quad (5)$$

here  $m_{\text{grav}}$  is the dynamical mass and  $m_{\text{evo}}$  the mass calculated by the stellar evolution code (so reduced by the mass loss). In case that a star experiences a supernova explosion we inject  $E_{\text{sn}} = 10^{51}$  ergs in the escaping particles by added this amount of energy to  $E_{\text{mech}}$ . The feedback efficiency parameter  $f_{\text{fb}}$  that accounts for the radiative losses is a free parameter, which we varied between  $f_{\text{fb}} = 0.01$  and 0.1. In order to track the rapid evolution caused by feedback we adopt a maximum time step for the gas particles of  $10^3$  years and after supernova events the maximum hydrodynamic time step is reduced to 20 years for 30k years in order to prevent time-stepping artefacts (a more elegant fix is described in Saitoh & Makino 2009; Durier & Dalla Vecchia 2011, but our approach has only a minor effect on the total running time). We summarize the various numerical parameters in Table 1.

### 2.3 Initial conditions

The simulated clusters in Table 2 are composed of a mixture of gas and stars (with  $N_{\star} = 1000$ ) distributed in a Plummer sphere. Stellar-stellar gravitational interactions are smoothed (Plummer smoothing) with a smoothing length  $0.001 \times R_{\text{scale}}$  and the interaction between gas particles and star particles are smoothed (using the SPH spline kernel) with the gas particle smoothing length. The stellar masses are assigned using a Salpeter IMF between 0.1

**Table 1.** Overview of the numerical parameters:  $\Delta t_{\text{gas}}$  is the maximum time step for hydrodynamics,  $\Delta t_{\text{fb}}$  defines the interval between feedback,  $\Delta t_{\text{bridge}}$  is the coupling time for mutual gas - star gravity kicks,  $t_{\text{sim}}$  is the total simulated time,  $\epsilon_{\text{soft}}$  is the gravitational smoothing adopted (for star-star interactions). Interactions with gas particles are smoothed using the local smoothing length),  $\eta$  is the usual N-body time step parameter for PhiGRAPE (Aarseth 2003) and  $\theta$  the Barnes & Hut (1986) opening angle for Octgrav.

parameter:	$\Delta t_{\text{gas}}$	$\Delta t_{\text{fb}}$	$\Delta t_{\text{bridge}}$	$t_{\text{sim}}$	$\epsilon_{\text{soft}}$	$\eta$	$\theta$
value:	0.001 Myr	0.04 Myr	0.04 Myr	30 Myr	0.001 $R_{\text{scale}}$	0.01	0.5

**Table 2.** Overview of initial conditions.

Model	$N_{\star}$	SFE	$M_{\star}$ ( $M_{\odot}$ )	$N_{\text{gas}}$	$M_{\text{gas}}$ ( $M_{\odot}$ )	$R_{\text{scl}}$ (pc)	$f_{\text{fb}}$	comment
A1	1000	0.05	355	100k	6740	0.5	0.1	
A2	1000	0.3	350-366	100k	815-855	0.5	0.1	×4
A3	1000	0.5	355	100k	355	0.5	0.1	
A4	1000	0.05	355	100k	6740	0.5	0.01	
A5	1000	0.3	355-366	100k	815-855	0.5	0.01	×4
A6	1000	0.5	355	100k	355	0.5	0.01	
A7	1000	0.3	355	100k	840	0.2	0.1	
A8	1000	0.3	355	100k	840	0.2	0.01	
A9	1000	0.3	355	100k	840	1.0	0.1	
A10	1000	0.3	355	100k	840	1.0	0.01	
B1	1000	0.05	355	100k	6740	0.5	0.1	sub-virialized
B2	1000	0.05	355	100k	6740	0.5	0.01	sub-virialized
B3	1000	0.05	355	100k	6740	1.	0.1	sub-virialized
B4	1000	0.05	355	100k	6740	1.	0.01	sub-virialized

and 100  $M_{\odot}$ , with the additional constraint that the most massive star in each cluster has a mass close to the median maximum mass for a cluster of this size ( $\approx 22 M_{\odot}$ ). This additional requirement is consistent with the expected maximum mass for small clusters (Weidner & Kroupa 2006; Portegies Zwart et al. 2010). The masses of the stars are assigned independently of the position in the cluster (constant SFE), so no initial mass segregation is imposed. Stellar collisions are not taken into account and during the simulation no gas accretion onto existing stars or new star formation is allowed. Note that any accretion of gas onto the stars would be very limited since we start from a smooth gas distribution and no cooling is included. Feedback induced star formation can also not occur in our approach, but is not very likely in the systems we simulate (see also Dale & Bonnell 2008).

In the series of calculations indicated with the letter ‘‘A’’ in Table 2 we explore the effect of the formation efficiency, the initial scale length and the feedback efficiency. We run models with a SFE of 0.05, 0.3 and 0.5. The initial Plummer radius of the initial conditions is either 0.1, 0.5 or 1.0 pc. Simulations with a feedback efficiency of  $f_{\text{fb}} = 0.01$  and 0.1 are performed. For small clusters the number of high mass stars can vary quite substantially between different realizations of the IMF, and we perform the model A2 and A5 with realizations of the IMF generated from different random seeds to examine this effect. We have performed additional simulations in which we varied the number of gas particles to tests that the results are independent of the resolution of the gas dynamics.

We also run a series of models in which the stars are dynamically cold (these models with a sub-virialized velocity dispersion are designated as model set ‘‘B’’ in Table 2). This

choice is motivated by the fact that the initial stellar velocity dispersion comes from turbulent velocities in the parent cloud (Geyer & Burkert 2001). The stellar component may form with a lower velocity dispersion than that required to be dynamically stable if the turbulence in the parent gas cloud has a scale length smaller than the Jeans length or if the gas cloud is (partially) pressure supported or partially supported by magnetic fields (Verschueren 1990). For this set of simulations we decrease the stellar velocities to 20% of the virialized values.

### 3 RESULTS

In Figure 3 we show the stellar and gas distribution of our ‘‘baseline’’ run A2 and its low feedback equivalent, run A5. At four moments in time we plot the stars and a cut through the  $z = 0$  plane of the gas density distribution. Looking at the first A2 frame (at 0.96 Myr) we see the early stages where stellar winds blow bouyant bubbles that rise in the potential of the star cluster. As the mechanical luminosity increases these bubbles grow until they start blowing away sizable fractions of the cluster medium and a free-flowing wind develops (4.37 Myr frame). The strong feedback proceeds to unbind most of the gas of the cluster. At approximately 9.5 Myr the cluster ISM has been blown away - the gas that is visible in this frame originates from the strong AGB wind of the heaviest progenitor (21  $M_{\odot}$ ). The supernova that explodes at 9.54 Myr leaves the cluster devoid of gas.

For the A5 simulation ( $f_{\text{fb}} = 0.01$ ) (both simulations use the same initial realizations for the IMF and stellar positions) the initial wind stages proceed less violently, with

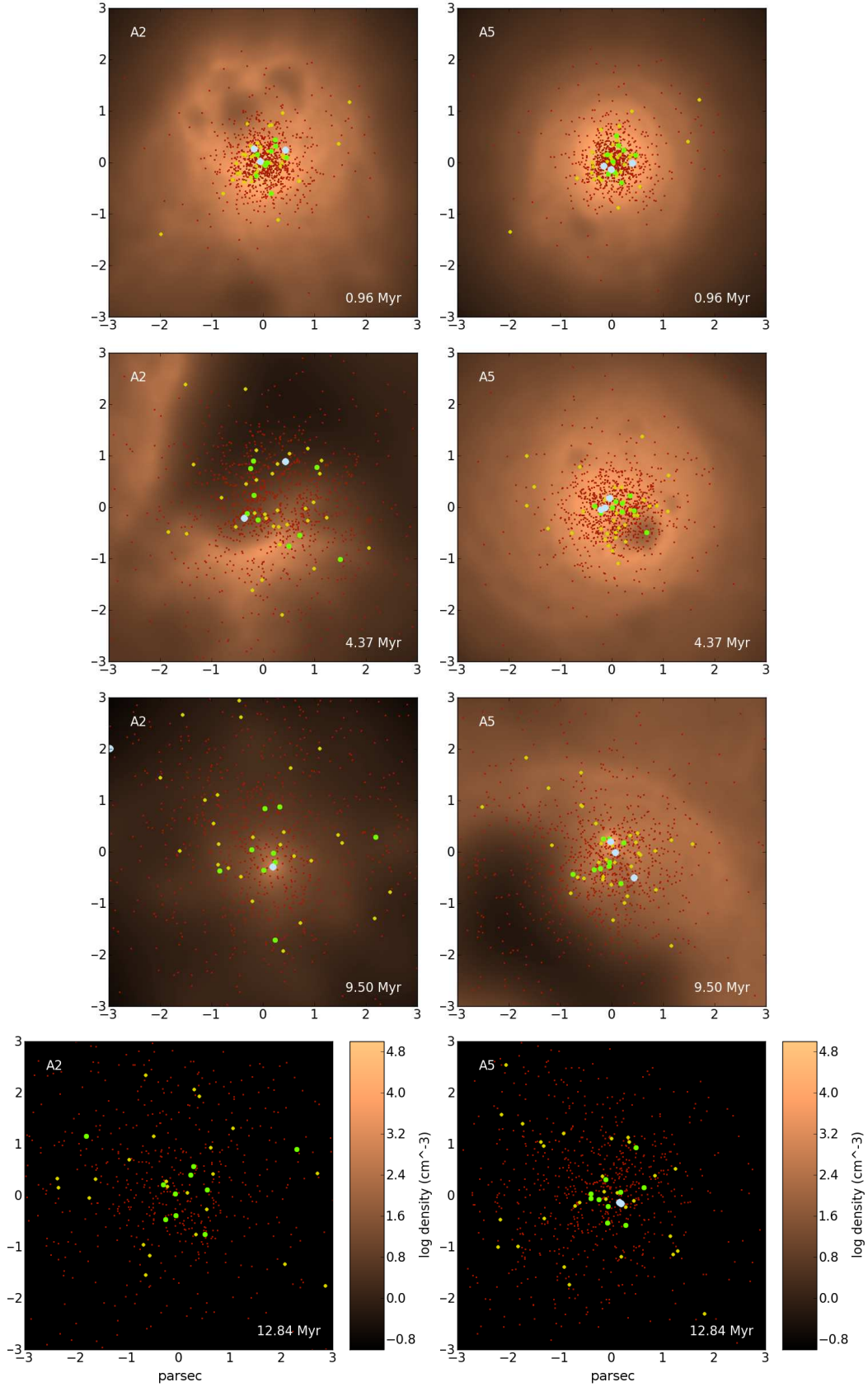


**Figure 3.** Stellar and gas distribution of the A2 and A5 run. Left panels show the gas and stellar distribution of the A2 run, Right panels of the A5 run. Snapshots are labelled with their time in the lower right corner. Shown as a density plot is a slice through the midplane of the gas density. Points show the stars in 4 mass groups:  $m_{\star} \leq 0.9 M_{\odot}$  (smallest red dots),  $0.9 M_{\odot} \leq m_{\star} \leq 2.5 M_{\odot}$  (intermediate yellow dots),  $2.5 M_{\odot} \leq m_{\star} \leq 10 M_{\odot}$  (intermediate green dots) and  $m_{\star} \geq 10 M_{\odot}$  (large light blue dots).



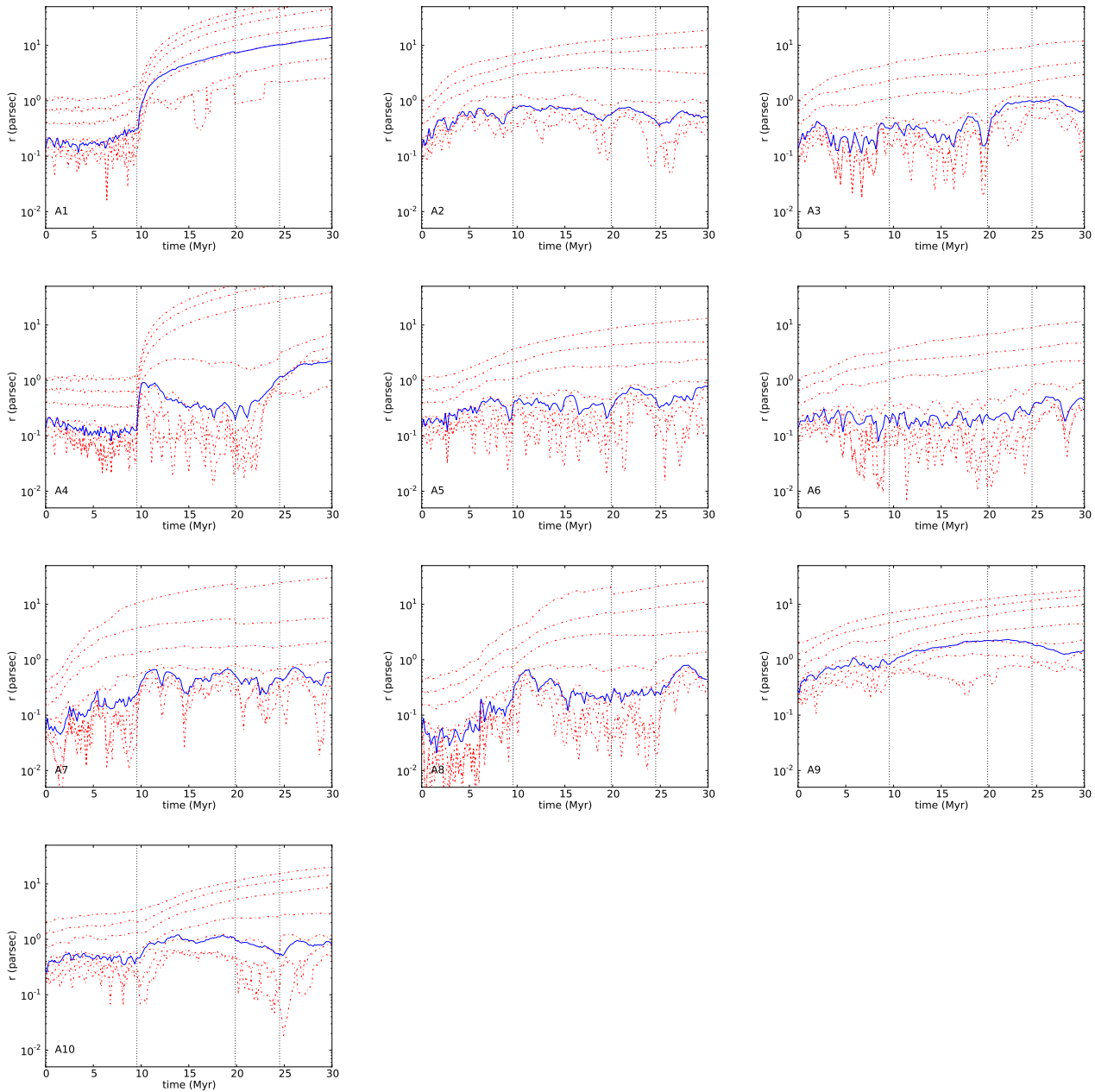


**Figure 4.** Lagrangian radii and core radius for runs A1-A10. Plotted in red dashed lines are the time evolution of the (0.02,0.05,0.1,0.2,0.5,0.75 and 0.9 ) Lagrangian mass radii of the stellar mass distribution. Blue line is the core radius. Vertical dotted lines indicate supernova events.

smaller bubbles (0.96 Myr), while a free-flowing wind does not develop (compare the frame at 4.37 Myr) until just before the supernova. The main difference between the A2 and A5 run is that most of the cluster gas remains present in the latter case, until the first supernova, at which stage the remaining gas is blown away. Just before the supernova the cluster is much more compact than in the A2 run.

The corresponding evolution of the Lagrangian radii and core radius and central gas density (of models A1-A10) is shown in Figure 4 and we plot in Figure 5 the (instantaneous) bound fraction of the gas and star component. For run A2, in the early phase (before 8 Myr) the gas is lost by

stellar winds. From the beginning of the simulation the gas starts to boil off vigorously under the influence of the stellar winds. The stellar distribution reacts by expanding. Within 3 Myr the core radius increases a factor  $\approx 2.5$  (within this time approx 2/3 of the gas is lost) and stays more or less constant thereafter. This is also visible in the maps of Fig. 3, where after the 4.37 Myr frame the stellar distribution remains qualitatively similar. Fig. 5 also shows that when the first supernova goes off, the gas in the cluster has already been completely removed. Later supernovae affect the stellar distribution very little. If we look at the bound fraction of stars shown in Figure 5 we see that  $\approx 60\%$  of the stars



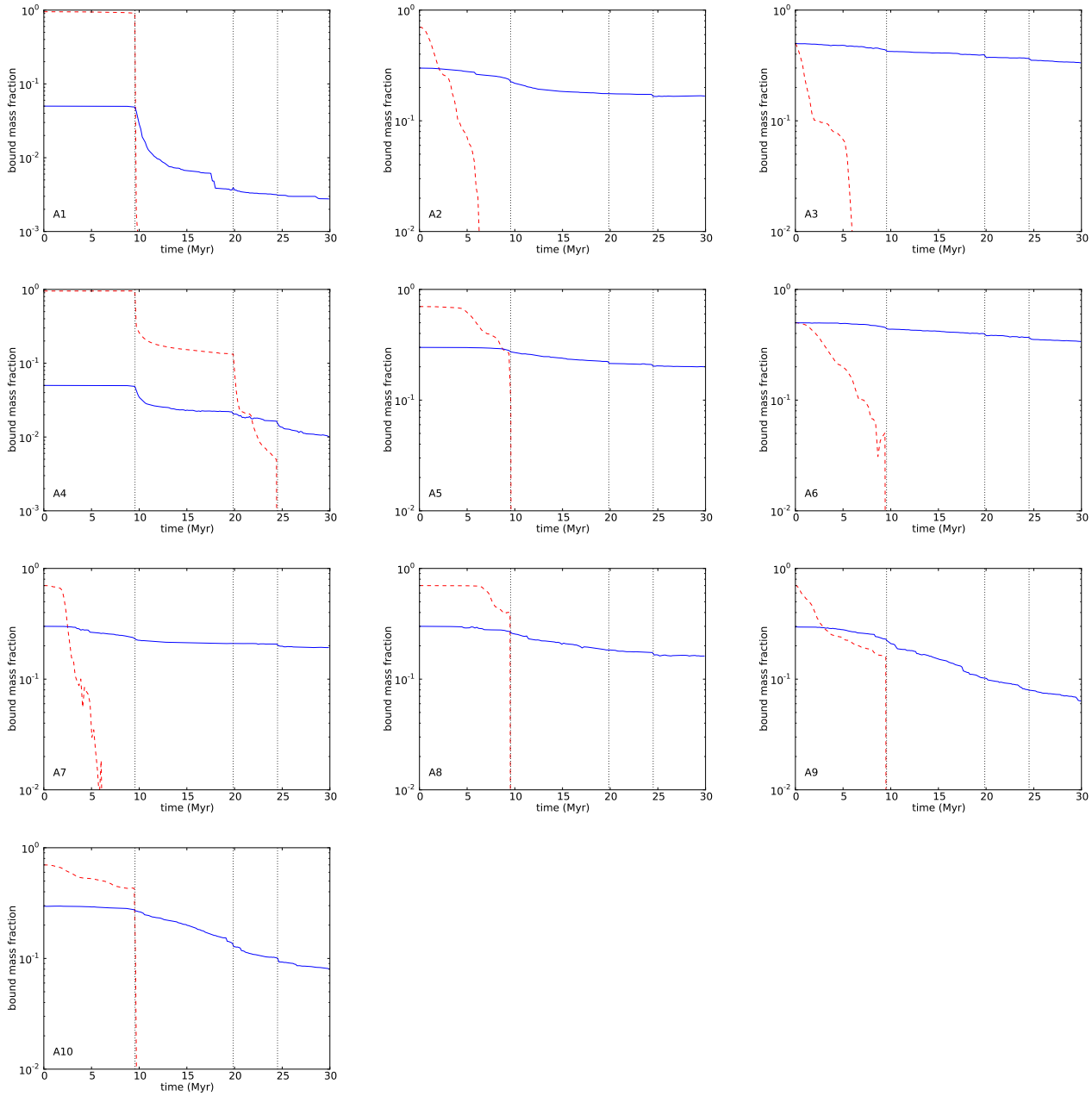


**Figure 5.** Stellar and gaseous bound mass fractions for runs A1-A10. Plotted is the bound stellar fraction (blue line) and the bound gaseous fraction (red dashed line) as fraction of the total initial system mass. Vertical lines indicate supernova events.

remain bound at the end of the simulation. The escape of stars happens mostly at the time of early gas loss, but with a noticeable delay. Note that the bound fraction plotted here and for other runs is an upper limit because this fraction is determined from the instantaneously bound stars (so at a particular point in time) and does not account for further unbinding by the escape of marginally unbound mass (this can account for part of the observed delay).

Comparing runs with different SFE (models A1,A2 and A3) we see that in the case of low SFE (run A1) most of the gas is retained up until the moment of the first supernova (see fig. 5). The gas completely unbinds because of the su-

pernova at 9.54 Myr, and the cluster is essentially dissolved immediately at that point. The high SFE case A3 is very similar to the A2 case. The initial gas loss may be somewhat steeper, but in this case (fig. 5) the loss of stars of the cluster proceeds more slowly. Looking at the evolution before the first SN, it is clear that the greater gas mass ( $20\times$  more) gives the A1 run greater resilience to the disturbance from stellar winds. Considering the escape of stars this leads to counteracting effects: when the fraction of gas is large, the loss of gas can more easily disturb the stellar distribution. However this loss happens initially much more slowly. In the A2 and A3 runs on the other hand, the gas starts to be

blown away right from the beginning, but the fraction of gas is small enough not to cause major disruption for the stellar distribution. When the supernova explodes, the gas of the A1 run is instantaneously removed, leading to the quick dissolution of most of the cluster. On the other hand, about 70% of the stars is retained in the A3 run.

If we look at the runs with the lower effective feedback strength (A4, A5 and A6), we see that in the  $SFE = 0.05$  case (A4) gas is still present after the first and second supernova. The stellar component reacts completely differently for the A4 run (compared with A1): in this case 50% of the stars remain bound initially, where only 10% remains in the A1 run. In the plot of the Lagrangian and core radii of run A4 (fig. 4) the core radius initially increases after the supernova, but then grows smaller again, as the cluster relaxes - markedly different from the continuing expansion in the A1 case. For the other two runs (A5 and A6), the lower effective feedback strength mainly results in a much less violent boil off compared with the high  $f_{fb}$  cases (e.g. A2 vs A5). Gas is still present at the time of the first supernova. For the stellar distribution this means that initially the stellar content remains intact (in particular the A5 run shows an almost constant bound fraction for the stellar component up until 9.5 Myr). The final bound stellar fractions and Lagrangian radii are qualitatively similar. The reason for this is that in both cases the total feedback energy is sufficiently large to unbind the cluster gas eventually. Much of the extra energy in the simulations with high feedback is carried away by the escaping gas. In the high feedback case gas loss by stellar winds is much more important, whereas in the low feedback case gas is driven out by supernovae. The final stellar distribution of the final cluster is little affected by the feedback efficiency over the range explored here, unless the gas fraction is very high.

### 3.1 Different realizations

For the low mass clusters we examine here different realizations of the stellar density distribution and the IMF will have very different masses and orbits for the heavy stars (and thus in the number, timing and location of supernovae) just due to low number statistics (the number of stars larger than  $10 M_{\odot}$  is  $\approx 4$ ). We have run additional realizations of the A2 and A5 simulations to quantify this effect. For the A2 runs the range in final stellar bound fractions is 50 – 70%, with the final core radii lying between 0.6 and 1.2 parsec. For the A5 runs we find similar ranges, 50 – 65% and 0.8 – 1.5 parsec. However if we compare the runs in more detail we see considerable differences. Two examples of this are given in figures 6 (Lagrangian and core radii) and 7 (bound fractions). The A2c run quickly loses 60% of its mass within 1.5 Myr, after which the gas loss slows down momentarily. This results in a stellar distribution that quickly expands, but then contracts again until the remaining gas is expelled. The A5d run seems to follow a similar pattern to the A5 run, if one compares the core radius. However if one looks more closely to the inner Lagrangian radii the A5d run is very different from the A5 run. In the latter case the (e.g.) 10% Lagrangian radius hovers around 0.2 parsec after 10 Myr, while in the A5d run it expands more than  $4\times$  further, to  $\approx 0.9$  parsec.

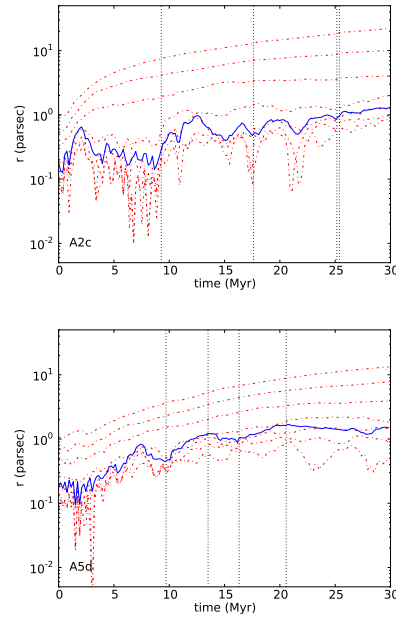


**Figure 6.** Lagrangian radii, core radius and central gas density for the alternative runs A2c and A5b. These differ from the corresponding runs in Fig. 4 only in the random seed that was used to sample the density distribution and IMF. Plotted in red dashed lines are the (0.02, 0.05, 0.1, 0.2, 0.5, 0.75 and 0.9) Lagrangian mass radii of the stellar mass distribution. Blue line is the core radius. Vertical dotted lines indicate supernova events.

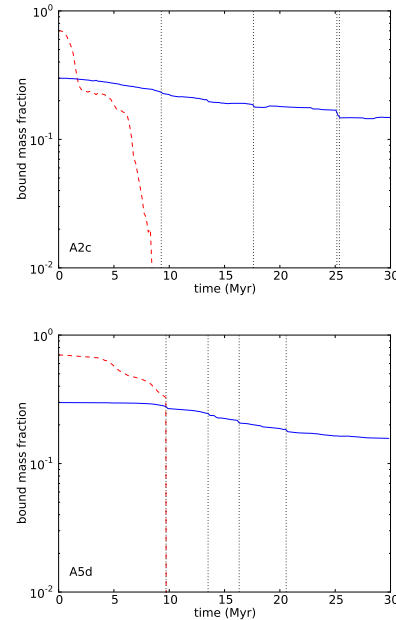


**Figure 7.** Stellar and gaseous bound mass fractions for the alternative runs A2c and A5b. These differ from the corresponding runs in Fig. 4 only in the random seed that was used to sample the density distribution and IMF. Plotted is the bound stellar fraction (blue line) and the bound gaseous fraction (red dashed lines) as fraction of the total initial system mass. Vertical lines indicate supernova events.

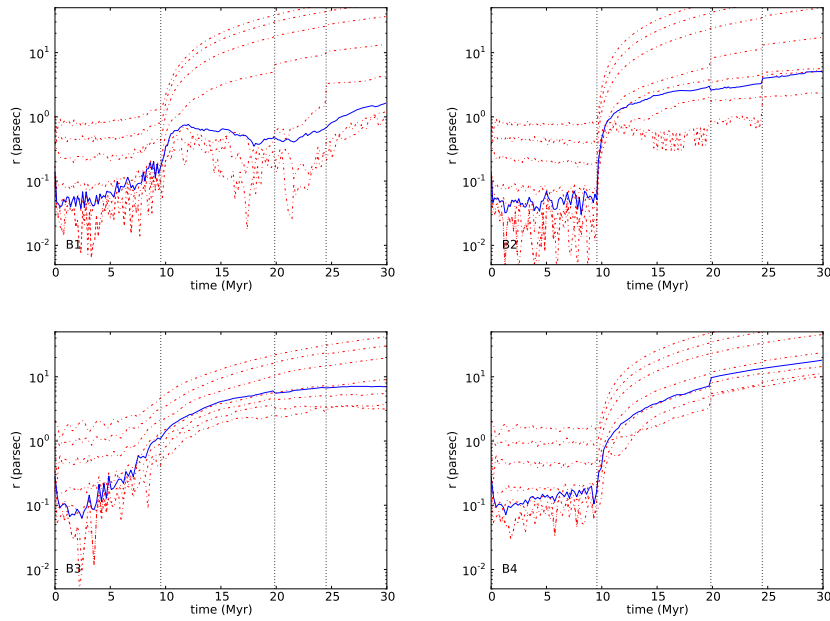


**Figure 8.** Lagrangian radii and core radius for runs B1-B4. Plotted in red dashed lines are the (0.02, 0.05, 0.1, 0.2, 0.5, 0.75 and 0.9 ) Lagrangian mass radii of the stellar mass distribution. Blue line is the core radius. Vertical dotted lines indicate supernova events.

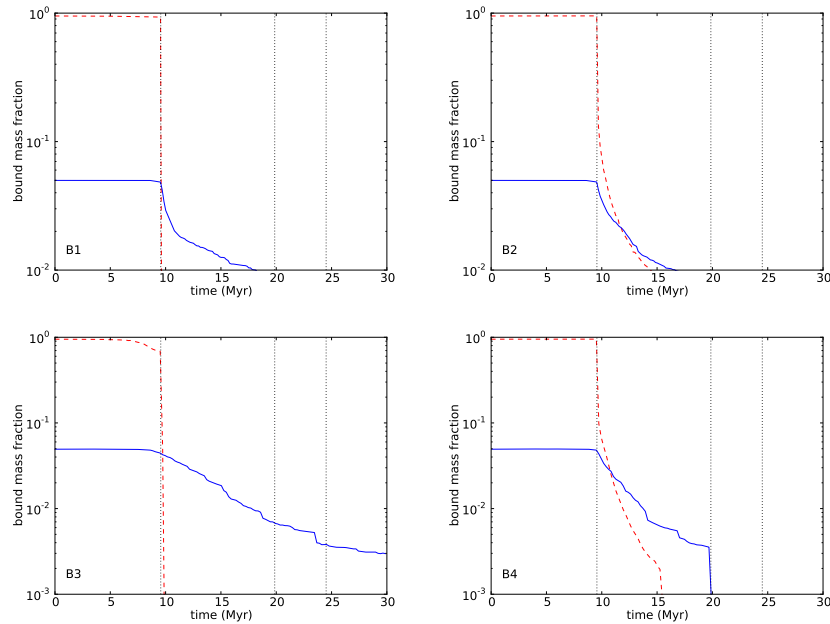


**Figure 9.** Stellar and gaseous bound mass fractions for runs B1-B4. Plotted is the bound stellar fraction (blue lines) and the bound gaseous fraction (red dashed lines) as fraction of the total initial system mass. Vertical lines indicate supernova events.

### 3.2 Sub-virial velocity dispersions

The time evolution of the Lagrangian radii and the bound fractions of the models with sub-virialized velocity dispersion are plotted in figures 8 and 9. Figure 8 shows that the stellar distributions quickly shrink compared to the virialized cases: e.g. for B1 the 0.5 Lagrangian radius drops roughly a factor 2 within less than 0.5 Myr. This collapse of the stellar distribution can increase the survival of the

stellar cluster, because the collapse increases the local SFE (Smith et al. 2011). The B1 model shows this effect, because compared with the A1 model it shows a much less drastic expansion of the core radius (fig. 8), although in the end the cluster still becomes completely unbound (fig. 9). However, surprisingly, if we look at the B2 model with a lower  $f_{\text{B}}$  (which is the sub-virialized version of the A4 run) we see exactly the opposite: in this case the cluster dissolves quickly, where as one may expect on the basis of the A1 and

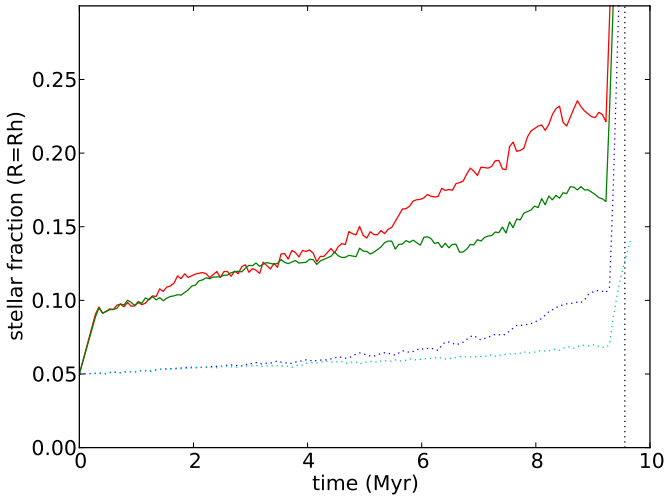


**Figure 10.** Stellar mass fraction at the (stellar) half mass radius. Plotted is the mass fraction at the half mass radius of the stellar distribution as a function of time (in the initial stages of the simulations) for the sub-virial velocity dispersions, runs B1 (red) and B2 (green), and their equivalent with full velocity dispersion A1 and A2 (blue and cyan dotted lines).

A4 run that the B2 run would dissolve much more slowly. Runs B3 and B4 show a similar pattern. The reason for this becomes clear if we examine figure 10, where we have plotted the stellar mass fraction (the ratio of stellar mass to total mass) within the stellar half mass radius as function of time up to the time of the first supernova. The dotted lines here show the A1 and A4 runs, while the drawn lines are the B1 and B2 runs. The B1 and B2 runs initially show an increase of a factor of 2 in stellar fraction (which is smaller than expected from the contraction of the half mass radius shown in fig. 8, indicating the gas distribution also contracts). After that they both show a slow increase, but crucially the B1 run shows a stronger increase to around 23% vs the B2 run. Although the increase is modest, it is probably the cause of the difference between the B1 and B2 run. This is consistent with the Baumgardt & Kroupa (2007) results, which show a very sensitive dependence of the bound fraction on SFE around a value of 0.25.

Note that Figure 10 shows that the stellar fraction of the A2 run is almost the initial value (SFE = 0.05). In this case the survival of the cluster after the first supernova is not due to a high stellar mass fraction, but due to the fact that not all gas is expelled (fig. 5). The effective SFE hence increases to  $SFE \approx 0.05 + 0.2$  (measured after 1 Myr) if one takes into account the gas that is not expelled. Hence the B1 and A2 run show an increased survivability due to completely different mechanisms: the B1 stellar component clears its environment of gas slowly through stellar winds and adapts to the slowly changing potential, while the stellar component of the A2 run is held together after the first supernova by remnant gas (in spite of this only being a very minor fraction of the initial gas component).

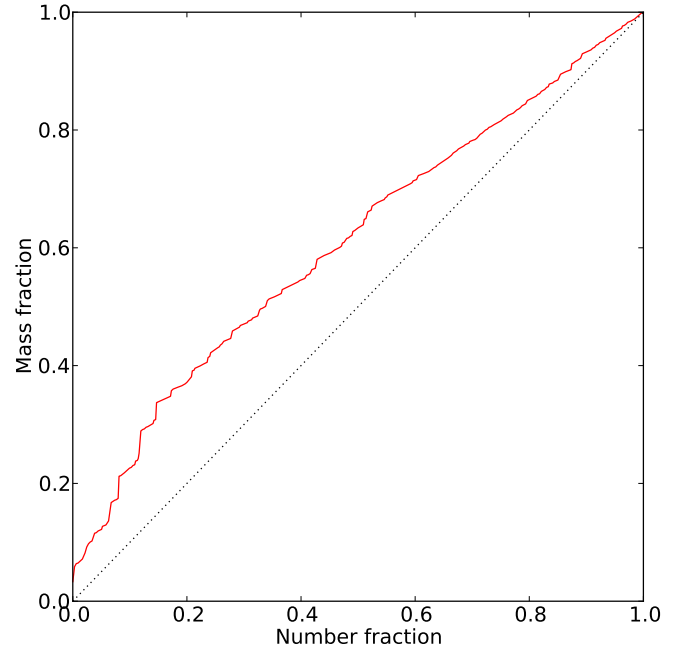


**Figure 11.** Mass fraction versus number fraction for the A2 run. Plotted is the mass fraction at given radii versus the number fraction at those same radii (at 30 Myr). A cluster without mass segregation would follow the dotted diagonal line. Following Converse & Stahler (2008) we take the area between the curve and the diagonal as a measure for the mass segregation (the Gini coefficient for the cluster).

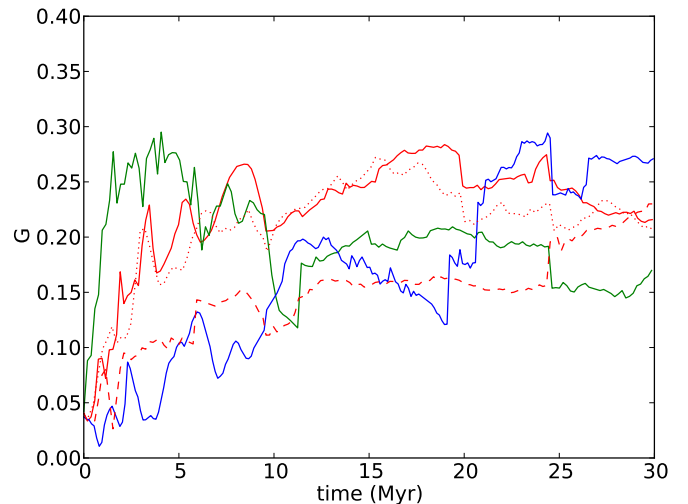


**Figure 12.** Plot of the Gini coefficient  $G$  as a function of time for different runs. The solid lines (red, green and blue) are runs with different initial half mass radius (A5, A8 and A10 runs respectively). Red dashed and dotted lines are the A2 run and A6 run.  $G$  is the area ( $\times 2$ ) between the graph of mass fraction vs number fraction and the diagonal (Fig. 11).

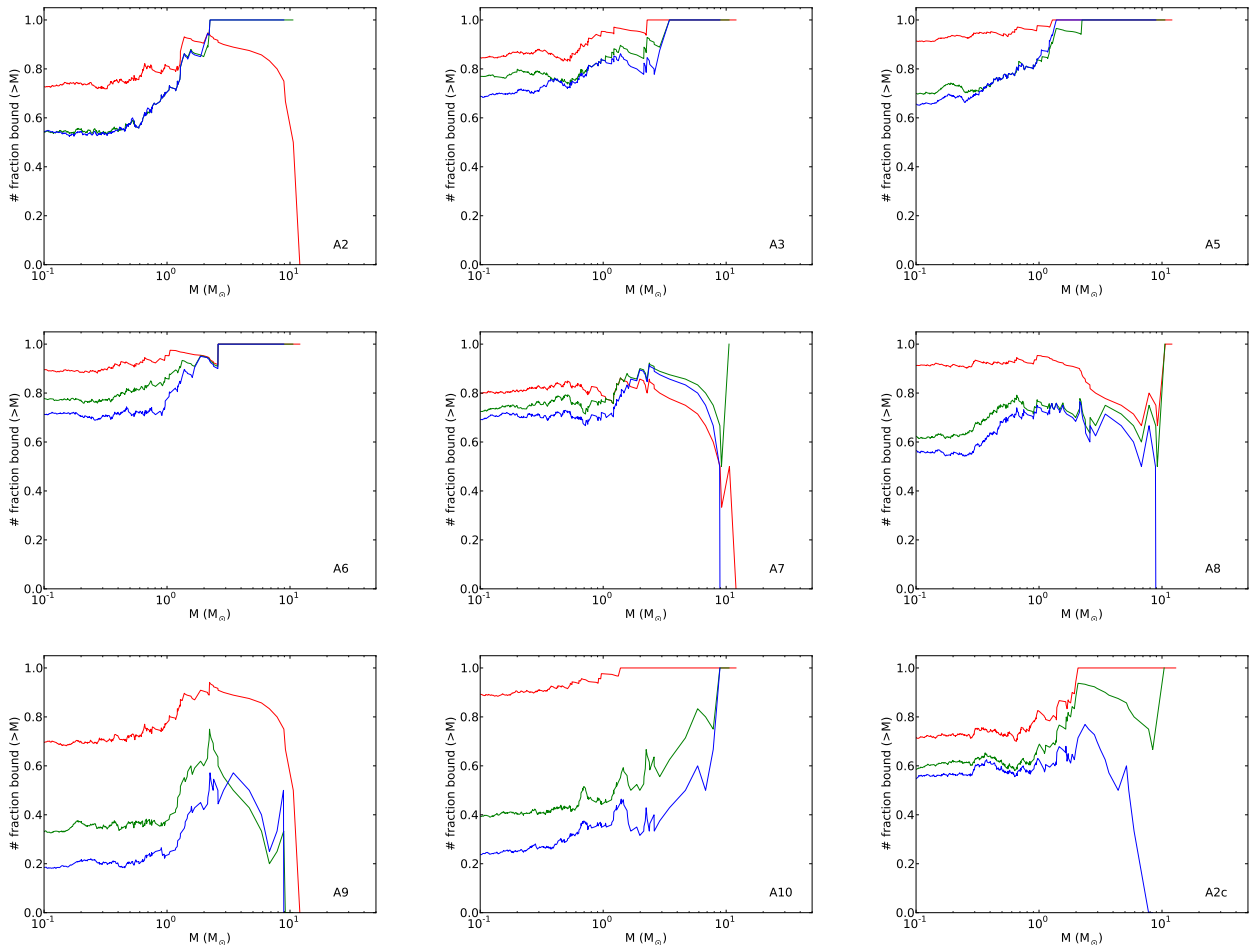


**Figure 13.** Cumulative bound number fraction as a function of mass. Plotted is, as a function of mass, the number fraction of stars heavier than that mass that are still bound at 10, 20 and 30 Myr. Shown are models from the basis set A1-A10 which result in a bound cluster (and the A2c run). Note that errors on these are not plotted - these increase from left to right from  $\approx 0.03$  to 1 for the right most point (because the right most point is based on a single data point).

### 3.3 Mass segregation and selective mass loss

Visual inspection of the maps such as those in figure 3 shows that the resulting remnant cluster are mass segregated. A useful way to quantify the mass segregation was presented by Converse & Stahler (2008) - they plotted the number fraction enclosed at given radii  $f_N$  against the enclosed mass fraction at those radii ( $f_M$ ). For mass segregated clusters (e.g. the Pleiades cluster in their paper)  $f_M$  will lie above  $f_N$  (an example of this procedure for our simulation A2 is given in fig. 11). A measure of the mass segregation can then be given by calculating the area between the graph of  $f_M$  and line of equality, which Converse & Stahler labeled the Gini coefficient  $G$  for the cluster.

We have plotted  $G$  for various runs as a function of time in figure 12. Looking at run A5 (solid red line) we see that in the beginning  $G$  rises quite quickly, within 5 Myr; after that  $G$  is more or less constant,  $G \approx 0.2 - 0.3$ . At the end of the simulations the cluster is hence in a mass segregated state. A similar picture emerges for run A6 (higher SFE, dotted line in Fig. 12) and for the higher feedback run (A2, dashed line). In the latter case  $G$  plateaus at a somewhat lower value. The other two drawn lines in figure 12 show the

runs with a higher and lower initial half mass radius, runs A10 and A8. As is expected in these cases the initial rise in  $G$  is slower (A10) and faster (A8) respectively. In all cases the final  $G$  settles around  $G \approx 0.2$ .

It is interesting to note that Converse & Stahler (2010) tried to model the Pleiades cluster in some detail by running pure N-body models, and they could not explain the observed  $G$  unless they started their simulations with a nonzero Gini coefficient of at least  $G \approx 0.2$ . Although our models do not try to specifically reproduce the Pleiades cluster, this seems consistent with Figure 12: Converse & Stahler (2010) started their simulation after the dispersal of gas and our models suggest that the nonzero  $G$  is a remnant of the fast evolution before gas dispersal. After gas dispersal the cluster is left in a much more dispersed state (the models of Converse & Stahler (2010) had virial radii  $\geq 3$  pc), with a  $G$  close to its present value. This suggests that the mass segregation in open clusters such as the Pleiades is not a result of the secular evolution of its present configuration, but a remnant of its embedded evolution stage.

The fact that mass segregation in our simulations occurs early in the embedded stage of the cluster evolution also

has a consequence for the stellar population of the remnant cluster. In Figure 13 we plot the number of stars heavier than a given mass which end up in the remnant cluster (i.e. are bound) as a function of star mass. The panels in figure 13 show that in most cases where there results a bound cluster, the heavier stars are preferentially retained (11 out of 15 runs show this pattern). A number of models do not show this pattern, especially A7 and A8. Note these clusters have drastically expanded. Note also that while the A7 and A8 runs do not show strong preferential retention of heavy stars, they do show mass segregation. It was previously noted (Boily & Kroupa 2003a) that simple virial theorem arguments underestimate the size of clusters after gas clearing, because there are always a number of stars in low velocity orbits. The preferential retention of heavy stars can be understood by noting that the mass segregation during the initial evolutionary stages happens because of the partitioning of stars in equal energy orbits: the heavy stars end up in low velocity orbits that are much more difficult to unbind. The heavy stars that are more easily retained may skew the IMFs that are derived from intermediate age clusters (as long as they are not observed in the initial stage) and this may result in an observable signature. Note that this could be tested for the Pleiades cluster, which is already known to have an excess of heavy stars in the center (Converse & Stahler 2010, e.g.).

### 3.4 Ratio of age and crossing time

Loosely bound associations can be distinguished from ‘true’ stellar clusters using limited observables by considering the ratio  $\Pi$  of age  $T_{\text{cl}}$  and the crossing time  $T_{\text{cross}}$  (Gieles & Portegies Zwart 2011):

$$\Pi \equiv T_{\text{cl}}/T_{\text{cross}} \quad (6)$$

where the  $T_{\text{cross}}$  is derived from

$$T_{\text{cross}} \approx 10 \left( \frac{R_{\text{eff}}^3}{GM} \right)^{1/2} \quad (7)$$

where the effective radius  $R_{\text{eff}}$  and mass  $M$  are easily estimated observable quantities. We determined the time evolution of  $\Pi$  using Eq. 7 for our simulations by measuring the  $R_{\text{eff}}$  and  $M$ . The resulting  $\Pi$  are plotted in figure 14. Note that we plot the  $\Pi$  for the case where we identify the cluster as being composed of all stars initially present or alternatively where only the bound stars are taken into account. The evolution of the  $\Pi$  of the clusters in Figure 14 can be understood as follows: in the beginning  $\Pi$  increases linearly but as the cluster is disturbed the  $\Pi$  ratio is “reset,” as the  $R_{\text{eff}}$  increases and the mass decreases. The tracks of our clusters end mostly with either a  $\Pi \approx 1$  (bound case) or with a very low  $\Pi$  in which case they should be dissolved (and no longer recognized as clusters). This is consistent with a possible explanation for the distribution of  $\Pi$  as a function of mass noted by (Gieles & Portegies Zwart 2011). They found that for young stellar associations both low and high  $\Pi$  values are present. While older stellar associations were exclusively found with  $\Pi \geq 1$  (and identified as proper clusters).

## 4 DISCUSSION

We performed simulations of relatively small clusters of 1000 stars with gas. Our simulations self-consistently take the dynamical evolution of the stars, their internal nuclear evolution and the dynamics of the embedded gas and the gas liberated by stellar evolution into account. Each of the physical domains, stellar dynamics, stellar evolution and hydrodynamics, is resolved with well tested numerical solvers which have been developed independently. The coupling between the domain-specific solvers is realized with the AMUSE framework, which enables us to couple codes written in a wide variety of languages in a homogeneous, transparent and self-consistent fashion. The final code has the form of a relatively simple Python script, which is general in its purpose of simulating embedded star clusters.

Our model clusters start with a mix of stars and gas in virial equilibrium at a hypothetical moment we call  $t = 0$ , at which all stars are on the zero-age main-sequence. The distribution of gas and stars was taken identical with a star-formation efficiency to control the relative mass fraction of the gas with respect to the stars. The feedback strength is parametrized using a parameter  $f_{\text{fb}}$ . We constrain the initial mass function to follow a Salpeter IMF with a minimum mass of  $0.1 M_{\odot}$  and an upper limit of  $100 M_{\odot}$ , but we fixed the maximum mass of a cluster star to  $22 M_{\odot}$  in order to prevent random fluctuations from the coincidental generation of a more massive star, because it turns out that the most massive star in our cluster dominates the out-gassing by its efficient segregation to the cluster center, the strong stellar wind and the moment the star experiences a supernova.

In our simulations a star formation efficiency  $\text{SFE} \geq 0.05$  results in a bound cluster, which is consistent with earlier simulations (e.g. Baumgardt & Kroupa 2007). However, a more detailed analysis of our simulation results reveals that the process is considerably more complicated. It turns out that the qualitative result with respect to final bound fraction can be approximated reasonably well with the parametrization of the SFE, but that the entire process is much richer. Baumgardt & Kroupa (2007) found that the most important parameters affecting the final cluster were the SFE and the gas loss timescale. Our simulations convincingly demonstrate that the simple parametrization in terms of the SFE and/or gas loss timescale is a gross oversimplification of the process of stellar-supported out-gassing of the young cluster. For example for the low feedback A4 run the initial supernova is not enough to disperse all cluster gas. After the first supernova 15% – 20% of the gas remains bound. From the standpoint of the dynamics of the stars this remnant gas increases the effective SFE. Hence the cluster initially relaxes (between 10-20 Myr) with a  $\approx 50\%$  bound fraction. Comparing with the Baumgardt & Kroupa results (Figure 1), we see that this is a reasonable value if we consider their  $\text{SFE} = 0.2$  curves: at these SFE a bound fraction of 50% is quite possible (even not accounting for any radial dependence of the gas loss). Further supernova events blow away the remaining gas, but do so only after the cluster has adapted itself dynamically. On the other hand, the B1 run shows if the gas loss occurs more gradually, the cluster can also adapt to gas loss (albeit in our simulations not enough to give rise to a bound cluster).

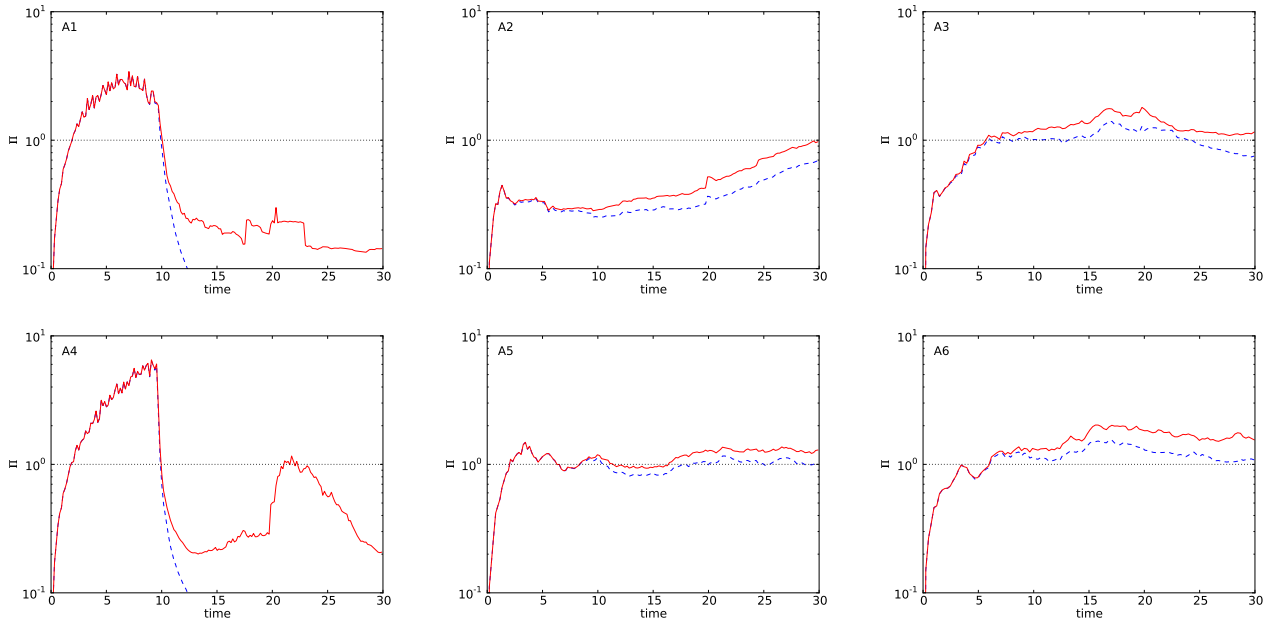


**Figure 14.** Plot of  $\Pi = \text{age}/T_{\text{cr}}$  for models A1-A6.  $T_{\text{cr}}$  is determined as in Eq. 6 where  $T_{\text{cr}}$  depends on  $R_{\text{eff}}$  and  $M$  (Gieles & Portegies Zwart 2011). Two different cases are plotted: taking into account bound stars only (red line) or alternatively including all the stars (blue dashed lines).

The time scale on which the gas is expelled cannot be described as a simple function, but depends on the distribution of the masses and positions of the stars, when they start blowing a strong stellar wind and the details regarding the moment of the supernovae (and the adopted feedback strength). Considering the wealth of variation in cluster parameters that result from this complex process the question remains why young star clusters show a relatively narrow range of properties, whereas we would naively expect a much wider range of cluster radii, and masses. At this moment we are unaware what key parameter may play a moderating role in the range of observables for young star clusters. Note that we did not take into account external limitations, such as the galactic tidal fields or the environment of the parent cloud.

In our simulations we do not model the stellar feedback fully self-consistently. The main uncertainties in our prescription concern the uncertainty in the efficiency of the coupling of the mechanical luminosity, the constraints of the numerical method and the lack of radiative feedback in our models. In future simulations we expect to deal with this latter point by resolving the radiative feedback using a radiative transfer code, but for now this remains part of the uncertainty encoded in the free parameter for the feedback strength we introduced in our models. This efficiency with which the output of stars couples to the surrounding gas may also depend on the mass of the star itself (Freyer et al. 2003, 2006), and on the state of the gas: the density, temperature but also on its clumpiness (an aspect we have not modeled). We do demonstrate, however, that the core radii and mass of the surviving cluster does not depend strongly on this efficiency parameter.

On the numerical side, it is well known that SPH shows relatively poor performance in the regime of explo-

sive shock waves: for example the peak densities are generally smoothed out. This could be important for the energy budget of the feedback, as the cooling happens mainly in these dense regions. On the other hand, the speed and post-shock states are well reproduced (Springel 2005; Pelupessy 2005) in SPH, so with the limitations we imposed on the details of the thermal evolution (the fact that we did not try to account self-consistently for the energy budget of the feedback) this has probably not a major impact. In future work, AMR employing Godunov-type solvers for the gas dynamics may be employed to improve this aspect. This would necessitate very high resolution simulations to reach a converged solution and the inclusion of much more physics to follow the (non-equilibrium) heating and cooling processes in the gas.

## 5 CONCLUSIONS

- We find that a  $\text{SFE} > 0.05$  is necessary to result in bound clusters.
- The actual dispersion of clusters at  $\text{SFE} = 0.05$  may occur gradual or sudden depending on the details of feedback. Before eventual dissolution, stable phases in the cluster evolution may occur if not all gas is expelled. Contributing to this is the increase in the effective SFE from the point of view of the stellar dynamics if feedback does not blow away all gas.
- We find that statistical variations can have a considerable effect on the internal structure of the remnant cluster.
- We find different modes of gas loss depending on the feedback coupling strength adopted. A high coupling strength results in a gradual loss of gas on timescales of  $\approx 5$  Myr. For the low feedback coupling stellar winds are not



able to disperse the gas: the timescale of gas loss in this case is very short (due to supernova explosions).

- More detailed modeling is necessary to put constraints on the energy budget and thermal evolution of the gas, especially for the early phases (where we do not take into account radiative feedback).

- During the embedded phase mass segregation can develop which persists after gas has been removed and the cluster has become less dense. This suggests that the observed mass segregation of open clusters such as the Pleiades is a remnant rather than the result of later secular evolution.

- Mass segregation followed by partial dissolution of the cluster tends to lead to an excess of heavy stars in the cluster. This is due to the fact that low velocity orbits are preferentially retained and the energy equipartition that forms the basis of mass segregation means that heavier stars preferentially populate the low velocity orbits.

- The dependence of the observed distribution of the ratio of the age of an association and its crossing time ( $\Pi$ ) is consistent with the “resetting of the  $\Pi$  clock” we find in our models. The short crossing times of young dense clusters increase due to stirring effect of mass loss. Unbound clusters are seen to have low  $\Pi$  values. These two effects together mean that clusters with both  $\Pi < 1$  and  $\Pi > 1$  are expected to be present as long as the gas dispersal and mass loss of young stars happens (before 30 Myr). This is consistent with what is observed (although more precise modeling should determine whether the observed distributions can be matched).

The fact that we find mass segregation and the preferential retention of high mass stars has consequences for the interpretation of cluster observations. In fact, observed clusters like the Pleiades show mass segregation. This mass segregation is usually attributed to the secular evolution in the pure N-body regime after the short lived embedded phase. For the Pleiades primordial mass segregation is necessary (Converse & Stahler 2008). Our models are able to reproduce the expected amount of initial mass segregation for the Pleiades cluster (although our models are not specifically build to reproduce the Pleiades). The fact that high mass stars are better able to withstand the disruptive effect of the loss of the natal cloud may lead to an excess number of unbound low mass stars in the vicinity of young clusters, which may be testable by expanding the search for cluster members to include kinematically unbound stars of the right age. We have demonstrated that it is important to consider both the embedded phase evolution and the gas clearing phase of cluster evolution together. Future studies will aim to include radiative feedback effects and should also take into account more realistic initial conditions for the cluster and gas distribution.

**Acknowledgements** This work was supported by the Netherlands Research Council NWO (grants #643.200.503, #639.073.803 and #614.061.608) and by the Netherlands Research School for Astronomy (NOVA).

## REFERENCES

Aarseth S. J., 2003, *Gravitational N-Body Simulations*  
 Adams F. C., 2000, *ApJ*, 542, 964  
 Barnes J., Hut P., 1986, *Nature*, 324, 446

Bastian N., Gieles M., Lamers H. J. G. L. M., Scheepmaker R. A., de Grijs R., 2005, *A&A*, 431, 905  
 Baumgardt H., Kroupa P., 2007, *MNRAS*, 380, 1589  
 Boily C. M., Kroupa P., 2003a, *MNRAS*, 338, 665  
 Boily C. M., Kroupa P., 2003b, *MNRAS*, 338, 673  
 Chen H., Ko C., 2009, *ApJ*, 698, 1659  
 Converse J. M., Stahler S. W., 2008, *ApJ*, 678, 431  
 Converse J. M., Stahler S. W., 2010, *MNRAS*, 405, 666  
 Dale J. E., Bonnell I. A., 2008, *MNRAS*, 391, 2  
 Dale J. E., Bonnell I. A., Clarke C. J., Bate M. R., 2005, *MNRAS*, 358, 291  
 Diaz-Miller R. I., Franco J., Shore S. N., 1998, *ApJ*, 501, 192  
 Duncan M. J., Levison H. F., Lee M. H., 1998, *AJ*, 116, 2067  
 Durier F., Dalla Vecchia C., 2011, *ArXiv e-prints*  
 Elmegreen B. G., Hunter D. A., 2010, *ApJ*, 712, 604  
 Evrard A. E., 1988, *MNRAS*, 235, 911  
 Fall S. M., Krumholz M. R., Matzner C. D., 2010, *ApJ*, 710, L142  
 Freyer T., Hensler G., Yorke H. W., 2003, *ApJ*, 594, 888  
 Freyer T., Hensler G., Yorke H. W., 2006, *ApJ*, 638, 262  
 Fujii M., Iwasawa M., Funato Y., Makino J., 2007, *PASJ*, 59, 1095  
 Gaburov E., Bédorf J., Portegies Zwart S., 2010, *Procedia Computer Science*, 1, 1119  
 Geyer M. P., Burkert A., 2001, *MNRAS*, 323, 988  
 Gieles M., Portegies Zwart S. F., 2011, *MNRAS*, 410, L6  
 Gieles M., Portegies Zwart S. F., Baumgardt H., Athanassoula E., Lamers H. J. G. L. M., Sipior M., Leenaarts J., 2006, *MNRAS*, 371, 793  
 Goodwin S. P., 2009, *Ap&SS*, 324, 259  
 Harfst S., Gualandris A., Merritt D., Spurzem R., Portegies Zwart S., Berczik P., 2007, *New Astronomy*, 12, 357  
 Hills J. G., 1980, *ApJ*, 235, 986  
 Hurley J. R., Pols O. R., Tout C. A., 2000, *MNRAS*, 315, 543  
 Kruijssen J. M. D., 2011, PhD thesis, Utrecht University, Utrecht, The Netherlands  
 Lada C. J., Lada E. A., 2003, *ARA&A*, 41, 57  
 Lada C. J., Margulis M., Dearborn D., 1984, *ApJ*, 285, 141  
 Larsen S. S., Brodie J. P., Huchra J. P., Forbes D. A., Grillmair C. J., 2001, *AJ*, 121, 2974  
 Leitherer C., Robert C., Drissen L., 1992, *ApJ*, 401, 596  
 Mathieu R. D., 1983, *ApJ*, 267, L97  
 Pelupessy F. I., 2005, PhD thesis, Leiden Observatory, Leiden University, P.O. Box 9513, 2300 RA Leiden, The Netherlands  
 Pelupessy F. I., van Elteren A., Marosvolgyi M., de Vries N., Portegies Zwart S., McMillan S., 2011, in preparation  
 Portegies Zwart S., McMillan S., Harfst S. e. a., 2009, *New Astronomy*, 14, 369  
 Portegies Zwart S. F., McMillan S. L. W., Gieles M., 2010, *ARA&A*, 48, 431  
 Prinja R. K., Barlow M. J., Howarth I. D., 1990, *ApJ*, 361, 607  
 Rodriguez-Gaspar J. A., Tenorio-Tagle G., Franco J., 1995, *ApJ*, 451, 210  
 Saitoh T. R., Makino J., 2009, *ApJ*, 697, L99  
 Saitoh T. R., Makino J., 2010, *PASJ*, 62, 301  
 Schweizer F., Seitzer P., 1998, *AJ*, 116, 2206

- Silich S. A., Franco J., Palous J., Tenorio-Tagle G., 1996, ApJ, 468, 722
- Smith R., Fellhauer M., Goodwin S., Assmann P., 2011, ArXiv e-prints
- Springel V., 2005, MNRAS, 364, 1105
- Vázquez-Semadeni E., Colín P., Gómez G. C., Ballesteros-Paredes J., Watson A. W., 2010, ApJ, 715, 1302
- Verschueren W., 1990, A&A, 234, 156
- Weidner C., Kroupa P., 2006, MNRAS, 365, 1333
- Wheeler J. C., Mazurek T. J., Sivaramakrishnan A., 1980, ApJ, 237, 781
- Williams J. P., McKee C. F., 1997, ApJ, 476, 166
- Wisdom J., Holman M., 1991, AJ, 102, 1528